MODELING OF CROSS-REGULATION IN CONVERTERS CONTAINING COUPLED INDUCTORS

Dragan Maksimović and Robert Erickson
ECE Department, University of Colorado
Boulder, CO 80301-0425
(303)492-4863

Carl Griesbach
Analog Systems
Morrison, CO
(303)697-4996

Abstract – **A general model of the multiple-winding coupled inductor is described, in which all parameters can be directly measured. This model is employed in a tutorial explanation of the mechanisms by which leakage inductances and effective turns ratios affect cross regulation and discontinuous conduction mode boundaries in a multiple-output converter. Three basic approaches to coupled-inductor design are compared: near-ideal coupling, practical moderate coupling, and the zero-ripple approach. Near-ideal coupling results in good cross-regulation even when some outputs become discontinuous; however, realization of near-ideal coupling may be difficult in practice, and the resulting circulating currents can also lead to increased output voltage ripples and reduced efficiency. The best cross regulation can be obtained via the zero-ripple approach with relatively loose coupling in applications where there is at least one output whose load current variations are relatively small so that all windings can always operate in the continuous conduction mode. The conclusions are supported by experimental results.**

1 Introduction

Several mechanisms degrade the cross regulation of multiple-output converters such as the 3-output forward converter shown in Fig. 1. Conduction losses of diodes, magnetics windings, and capacitor esr cause the output voltages to vary with the load currents. The effects of conduction losses on cross regulation can be predicted using averaged models, as in [1, 2], for example. Transformer leakage inductances cause variations in the diode conduction times, which is another factor that introduces some dependence of the output voltages on the load currents [3]. When an output enters the discontinuous conduction mode (DCM), its voltage ceases to track the other output voltages, and wide voltage swings occur. Use of coupled inductors in multiple-output buck-derived converters is a well known and conventional method for improvement of cross regulation [4]. The degree of cross regulation obtained depends on the coupling between windings and on the effective turns ratios between the windings. These parameters strongly affect the current ripple in each winding, and hence also the DCM boundaries. Mismatches in the turns ratios, especially in the case when the windings are tightly coupled, can lead to large circulating currents, discontinuous conduction mode, increased output voltage ripple, and degradation of efficiency and cross regulation. Since practical coupled inductors contain (possibly distributed) air gaps, near-ideal coupling is also difficult to obtain in practice. Complete understanding of the influence of coupled inductor construction on cross regulation is hampered by lack of a practical and valid model of multiple-winding coupled inductors, and by the complexity of multiple-output circuit behavior. The objective of this paper is to describe a suitable coupled-inductor model, and to explain its predictions in a tutorial manner.

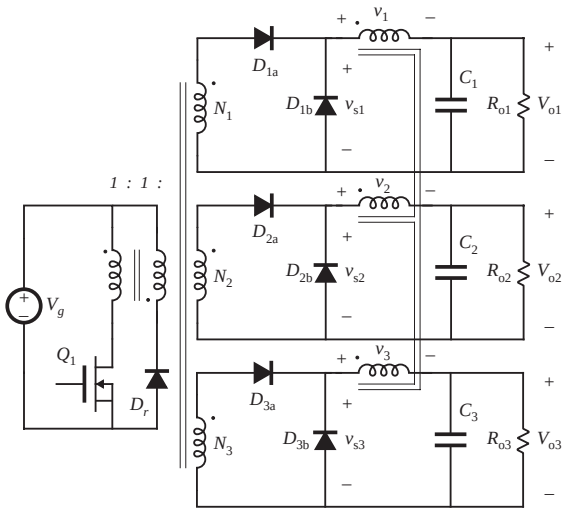

Figure 1: A three-output forward converter with coupled inductors.

A valid general model of the n-winding coupled inductor, in which all parameters can be directly measured, is introduced in Section 2. In Section 3, this model is used to show how leakage inductances and effective turns ratios affect DCM boundaries and cross-regulation. Three approaches to coupled inductor design are compared in Section 4: near-ideal coupling, practical moderate coupling, and the zero-ripple approach. The key points are validated by experiments.

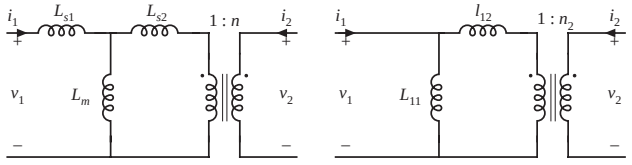

Figure 2: T-model (a) and the cantilever model (b) of a two-winding transformer.

2 The Extended Cantilever Model

The magnetics of multiple-output converters typically contain several windings having moderate to good coupling. The well-known general model for multiple-winding coupled inductors includes self-inductances L_{jj} and mutual inductances $L_{ij} = L_{ji}$. The parameters in this model can be measured directly and the model is also supported by simulation tools such as Spice. Unfortunately, the model based on self and mutual inductances is not well suited when the windings are well coupled and when leakage inductances determine behavior of the magnetic device, which is usually the case. Determination of the values of leakage inductances from the self and mutual inductances is practically impossible in the well-coupled case because of the numerically ill-conditioned nature of the computations. As a result, even small errors in the values of self and mutual inductances result in large errors in the values of leakage inductances. In this section, we describe a general circuit model for multiple-winding coupled inductors where the leakage inductances are directly exposed and where all parameters can be directly measured.

In the general n-winding case, $n(n+1)/2$ parameters are necessary. It is well known that the simple model containing an ideal transformer and leakage inductances in series with each winding is insufficient to describe such devices, and that leakage inductances which model the coupling of each winding to every other winding are necessary [1]. Previous authors ([5, 6], and others) have dealt with the complexity of this general model by developing reduced models based on physical and geometrical arguments. In general, however, such reduced models may not be able to predict observed behavior. Also, physical and geometrical arguments are difficult to apply to many cases of interest, such as toriodal geometries, especially when the magnetic device contains (possibly distributed) air-gaps.

Consider the basic T model of the two winding transformer shown in Fig. 2(a). The model contains four parameters: two leakage inductances, a magnetizing inductance, and a turns ratio. However, only three parameters are needed to describe the two winding transformer, and hence one of the T-model parameters can be chosen arbitrarily [1, 5, 6]. When one of the leakage inductances is chosen to be zero, then the cantilever model of Fig. 1(b) is obtained. This simple model contains three parameters and is well suited to modeling transformers having moderate or good coupling. We propose to extend the cantilever model of Fig. 1(b) to n windings. As an example, Fig. 3 shows the four-winding *extended cantilever model*. This model contains the correct number of parameters, and hence is completely general. It also has the advantage that each

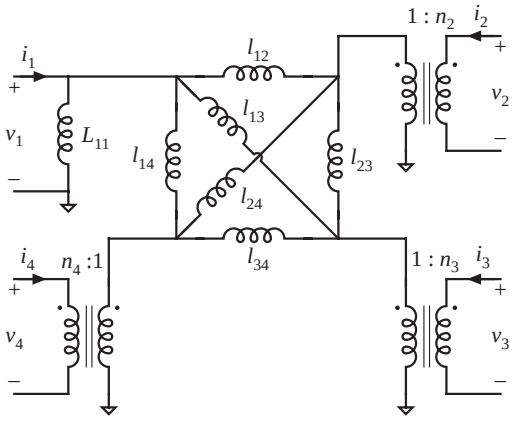

Figure 3: Extended cantilever model for 4 coupled inductors.

parameter in the model can be *measured simply and directly*. The shunt inductance L_{11} is equal to the self inductance of winding 1. The effective turns ratios n_j are found by driving winding 1 with a voltage source, and measuring the open-circuit voltages v_j at the other windings,

$$n_j = \left\| \frac{v_j}{v_1} \right\| . \tag{1}$$

Each series leakage inductance l_{ij} is measured by an experiment involving driving the i^{th} winding with a voltage source of angular frequency ω, shorting all other windings, and measuring the current i_j induced in the j^{th} short-circuited winding,

$$l_{ij} = \frac{1}{\omega} \frac{1}{n_i n_j} \left\| \frac{v_i}{i_j} \right\| . \tag{2}$$

The extended cantilever model can be used as a tool to characterize multiple-winding transformers and coupled inductors in a wide range of applications. In this paper, the model is used for analysis of cross-regulation in converters that contain coupled inductors. The model has also been applied to analysis and simulation of power-factor correctors based on coupled-inductor converters [8].

3 Discontinuous Conduction Mode in Multiple-Output Converters with Coupled Inductors

Consider a multiple-output converter, such as the forward converter of Fig. 1. If all outputs operate in the continuous conduction mode (CCM), steady-state cross-regulation is determined by conduction losses and by unequal diode conduction times due to transformer leakages and unequal device turn-on/turn-off times. When an output enters the discontinuous conduction mode (DCM), its voltage ceases to track the other output voltages, and cross regulation is degraded further because the output voltage in DCM is strongly load dependent.

In this section, we show how the extended cantilever models can be used to determine boundaries of operation in the CCM, and the voltage conversion ratio when one of the outputs operates in the DCM. In the analysis that follows, we assume that conduction losses and the effects of unequal diode conduction times are small. Under these idealized conditions,

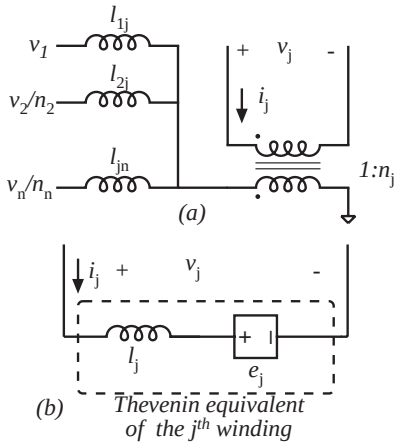

Figure 4: Derivation of the Thevenin equivalent circuit for the j^{th} winding.

cross-regulation is perfect as long as all outputs operate in the continuous conduction mode.

Suppose that all outputs operate in the continuous conduction mode, and that we vary the load only on the j^{th} output. To determine the CCM/DCM boundary for the j^{th} output, it is convenient to construct a Thevenin equivalent circuit for the j^{th} winding of the coupled inductor as shown in Fig. 4. The Thevenin equivalent circuit consists of an inductance l_j in series with a dependent voltage source e_j, which is a linear combination of all other winding voltages:

$$e_j = \sum_{\substack{k=1,\ldots,n \\ k\neq j}} a_{jk} v_k \,. \tag{3}$$

Using the part of the extended cantilever model shown in Fig. 4(b), the parameters in the Thevenin equivalent can be obtained in terms of the cantilever parameters:

$$\frac{1}{l_j} = \frac{1}{n_j^2} \sum_{\substack{k=1,\ldots,n \\ k\neq j}} \frac{1}{l_{jk}} \,, \tag{4}$$

$$a_{jk} = \frac{1}{n_j n_k} \frac{l_j}{l_{jk}} \,. \tag{5}$$

It is interesting to note that the parameters of the Thevenin equivalent have a simple physical interpretation and can also be measured directly: the series inductance l_j is the inductance of the j^{th} winding with all other windings short circuited, while the coefficient a_{jk} is equal to the voltage transfer ratio v_j/v_k when all windings (other than the j^{th} and the k^{th}) are short circuited.

Once the parameters in the Thevenin equivalent circuit are determined, the equivalent circuit for the j^{th} output shown in Fig. 5 can be used to find the CCM/DCM boundary condition.

Under the assumption that all outputs operate in the CCM, and that conduction losses and the effects of transformer leakages can be neglected, the voltage waveforms of all windings are proportional,

$$\frac{v_1}{N_1} = \frac{v_2}{N_2} = \cdots = \frac{v_n}{N_n} \tag{6}$$

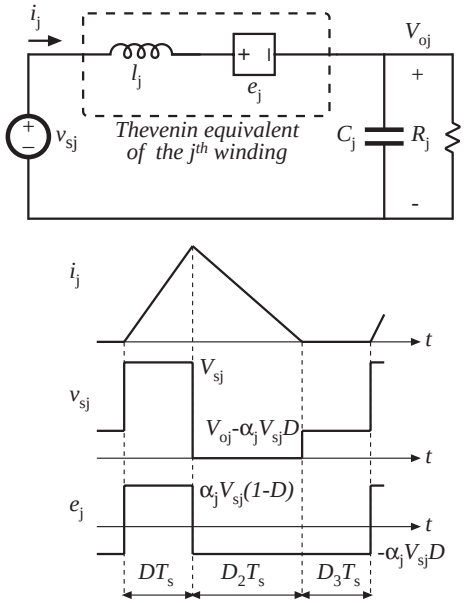

Figure 5: Equivalent circuit model of the j^{th} winding and waveforms used in the analysis of the discontinuous conduction mode.

As a result, the Thevenin source e_j is proportional to the winding voltage v_j,

$$e_j = \alpha_j v_j \,, \tag{7}$$

where the constant α_j can be found as:

$$\alpha_j = \sum_{\substack{k=1,\ldots,n \\ k\neq j}} a_{jk} \frac{N_j}{N_k} \,. \tag{8}$$

In the CCM, the slopes of the current i_j are:

$$l_j \frac{di_j}{dt} = \begin{cases} (V_{sj} - V_{oj})(1-\alpha_j), & 0 \le t \le DT_s \\ -V_{oj}(1-\alpha_j), & DT_s < t \le T_s \end{cases} \tag{9}$$

which yields the current ripple

$$\Delta i_j = \frac{V_{oj}|1-\alpha_j|}{2 l_j f_s}(1-D) \,. \tag{10}$$

The condition $V_{oj}/R_j \ge \Delta i_j$ for operation of the j^{th} output in the CCM becomes:

$$k_j \ge (1-D) \,, \tag{11}$$

where

$$k_j = \frac{2 l_j f_s}{R_j} \frac{1}{|1-\alpha_j|} = \frac{K_j}{|1-\alpha_j|} \,, \tag{12}$$

is a constant that plays the same role as the constant $K = 2Lf_s/R$ commonly used in DCM analysis of single-output converters.

In the case of uncoupled inductors, $\alpha_j = 0$, $l_j = L_j$, $k_j = K_j$, and the CCM condition (11) reduces to the well-known CCM condition for the single-output buck converter. It can be observed that non-zero α_j due to inductor coupling extends the load range in CCM. In particular, if $\alpha_j = 1$ and $l_j > 0$,

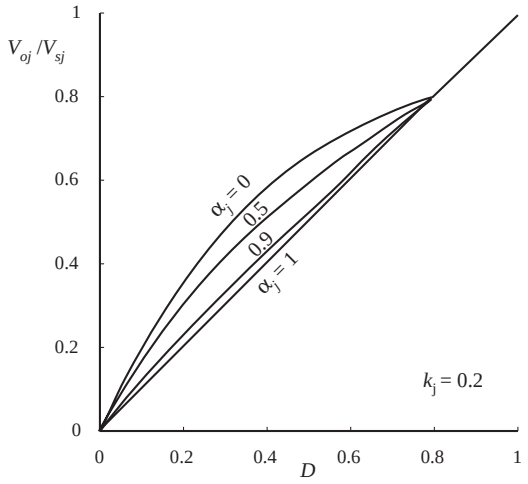

Figure 6: DC conversion ratio V_{oj}/V_{sj} for the j^{th} output. The output operates in the DCM for $D < 1 - k_j = 0.8$.

the j^{th} output operates in the CCM for any load, and the current ripple is ideally zero. If $\alpha_j > 1$, "reverse" ripple (with negative slope during the time when the main switch is on) would be observed in the j^{th} winding current.

Typical waveforms for operation of the j^{th} output in DCM are shown in Fig. 5. The slopes of the current i_j are:

$$l_j \frac{di_j}{dt} = \begin{cases} V_{sj} - \alpha_j V_{sj}(1-D) - V_{oj}, & 0 \le t \le DT_s \\ -(V_{oj} - \alpha_j V_{sj} D), & DT_s < t \le (D+D_2)T_s \\ 0, & (D+D_2)T_s \le t \le T_s \end{cases} \tag{13}$$

The charge-balance and the volt-second balance equations applied to the waveforms shown in Fig. 5 yield the conversion ratio V_{oj}/V_{sj} for the case when the j^{th} output operates in the DCM, $0 \le \alpha_j \le 1$, and all other outputs are in the CCM:

$$\frac{V_{oj}}{V_{sj}} = \frac{2\,(1-(1-D)\alpha_j)}{1 - \frac{k_j \alpha_j}{D} + \left(1 + \frac{k_j \alpha_j}{D}\right)\sqrt{1 + \frac{4k_j(1-\alpha_j)}{(D+k_j\alpha_j)^2}}}. \tag{14}$$

If the j^{th} inductor is uncoupled, $\alpha_j = 0$, and the expression (14) for the voltage conversion ratio reduces to the well-known DCM conversion ratio of buck converters. If $\alpha_j = 1$, $V_{oj}/V_{sj} = D$, which is exactly the same as the ideal CCM conversion ratio. Fig. 6 shows the conversion ratio as a function of the duty ratio D for constant k_j and several values of α_j. The conclusion is that non-zero α_j due to inductor coupling not only extends the load range in CCM, as shown by (11), but it also keeps the DCM conversion ratio closer to the conversion ratio in CCM, thus improving cross regulation, as shown by (14).

4 Design Approaches

In this section, specific design approaches are discussed using the results of Section 3. The experimental three-output converter shown in Fig. 7 is used to illustrate the discussion. In the experimental circuit, the main output (output 1) is regulated at $V_{o1} = 5.1$V and the auxiliary outputs (outputs 2 and 3) are unregulated. This circuit is constructed so that

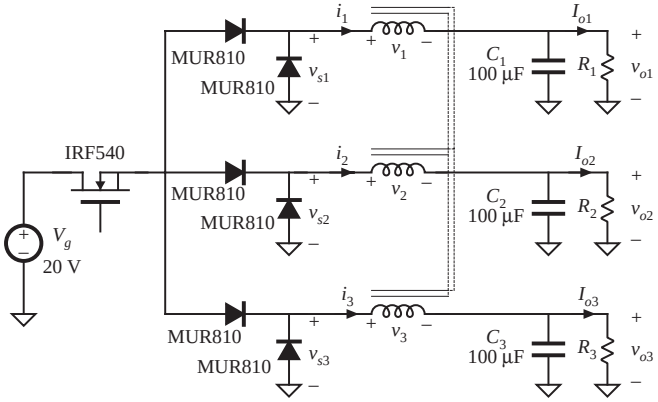

Figure 7: Experimental three-output converter. V_{o1} is close-loop regulated at 5.1V. The switching frequency is $f_s = 50$kHz.

	n_2	n_3	l_{12}	l_{13}	l_{23}
design #1	1.004	0.919	0.36μH	21.3μH	16.4μH
design #2	0.997	0.994	0.36μH	96.2μH	84.1μH

Table 1: Parameters of the three-winding cantilever model for the coupled-inductor designs shown in Fig. 8. In both designs the self-inductance of winding W1 is $L_{11} = 88\mu$H.

experimental verification of cross-regulation issues related to the coupled-inductor design can be separated from the effects of transformer leakage inductances that would occur in a practical converter with isolation transformer.

The experimental coupled inductors are wound using #20 AWG wire on a Magnetics Inc. 58254 high flux density powdered iron toriodal core. The extended cantilever model parameters have been measured for two different coupled-inductor designs shown in Fig. 8.

In the design #1 shown in Fig. 8(a), all three windings have the same number of turns (24). Windings W1 and W2 are bifilar, while winding W3 is wound on top of the windings W2 and W3. The measured cantilever model parameters for the design #1 are shown in Table 4. The bifilar windings are tightly coupled: l_{12} is very small, and the effective turns ratio n_2 is essentially equal to the physical turns ratio $n_2 \approx 1$. Winding W3 is coupled moderately well to the windings W1 and W2. As a result, series inductances l_{13} and l_{23} are significantly larger than l_{12}, and the effective turns ratio n_3 is smaller than the physical turns ratio, $n_3 = 0.92 < 1$.

In the design #2 shown in Fig. 8(b), windings W1 and W2 are bifilar with the same number of turns (24), while winding W3 has 28 turns wound on the opposite side of the toriod. The measured cantilever model parameters for the design #2 are also shown in Table 4. The bifilar windings are tightly coupled as in the design #1. Winding W3 is loosely coupled to windings 1 and 2 so that the series leakage inductances l_{13} and l_{23} are relatively large. The number of turns in winding W3 is increased to 28 (compared to 24 turns on W1 and W2), in order to have the effective turns ratio n_3 close to 1.

The parameters of the Thevenin equivalent used in Section 3 to determine boundaries of operation in the CCM can be found

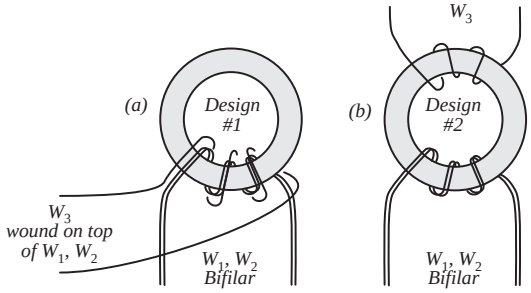

Figure 8: Two coupled-inductor designs tested in the experimental circuit of Fig. 7. In the design #1, windings W1, W2 and W3 have 24 turns each. In the design #2, windings W1, W2 have 24 turns each, winding W3 has 28 turns.

	l_2	α_2	l_3	α_3
design #1	0.358μH	1.006	7.81μH	0.919
design #2	0.384μH	0.990	44.3μH	0.994

Table 2: CCM/DCM analysis parameters l_j and α_j for the two coupled-inductor designs of Fig. 8.

using (4), (5) and (8). For example, (4) gives l_3 as the parallel combination of l_{13} and l_{23} referred to winding W3:

$$l_3 = n_3^2(l_{13}||l_{23}) = 7.81\mu H\,, \tag{15}$$

using the design #1 parameter values. The Thevenin source e_3 is found using (5) as:

$$\begin{aligned} e_3 &= n_3\frac{l_{23}}{l_{13}+l_{23}}v_1 + \frac{n_3}{n_2}\frac{l_{13}}{l_{13}+l_{23}}v_2 = & (16)\\ &= a_{31}v_1 + a_{32}v_2 = & (17)\\ &= 0.400\,v_1 + 0.519\,v_2\,. & (18)\end{aligned}$$

Finally, since $N_1 = N_2 = N_3$, the coefficient α_3 in (8) is

$$\alpha_3 = a_{31} + a_{32} = 0.919\,. \tag{19}$$

Numerical values of l_j, α_j parameters in the two designs are summarized in Table 4.

The experimental circuit of Fig. 7 and the two coupled-inductor designs of Fig. 8 are used to illustrate the discussion of three approaches to coupled-inductor design.

4.1 Near-Ideal Coupling

In the case of near-ideal coupling, the series leakage inductances l_{jk} in the extended cantilever model are very small and the inductance l_j in the Thevenin equivalent circuit of the j^{th} winding is therefore very small. As a result, even slight mismatch of winding voltages imposed on the coupled inductor by the converter causes significant current spikes ("circulating currents"). The mismatch in winding voltages is caused by second-order effects such as small output capacitor voltage ripples, conduction losses, and unequal diode turn-on/turn-off times. The winding current waveforms can differ substantially from the familiar triangular shape. For example, the waveforms of Fig. 9 show current spikes in the current i_2 of winding W2, which is tightly coupled to the winding W1. These

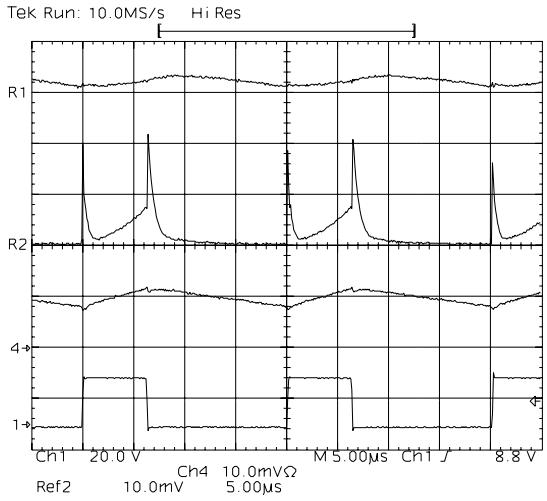

Figure 9: Waveforms in the experimental circuit using the coupled-inductor design #2; top-to-bottom: (R1) i_3 (100mA/div); (R2) i_2 (100mA/div); (4) i_1 (2A/div); (1) v_{s1} (20V/div). Operating conditions: $V_{o1} = 5.1$V, $I_{o1} = 2$A, $V_{o2} = 5.7$V, $I_{o2} = 20$mA, $V_{o3} = 5.66$V, $I_{o3} = 20$mA.

current spikes are due to the unequal diode turn-on/turn-off times, and are not predicted by the analysis of Section 3. In the case of near-ideal coupling, however, effective turns ratios are close to the turns ratios of the physical windings. As a result, α_j is very close to 1, which indicates that the winding voltage waveforms track closely, leading to good cross-regulation even in DCM.

4.2 Moderate Coupling

In this case, which is commonly obtained in practice, the series inductances are moderate in value and the effective turns ratios differ somewhat from the turns ratios of the physical windings. The winding currents typically exhibit triangular waveforms, and the analysis of DCM boundaries in Section 3 yields reasonably accurate predictions. Because the leakage inductances are larger, the winding current ripples are reduced and outputs are less likely to operate in the discontinuous conduction mode (as opposed to the near-ideal coupling case). However, the winding voltage waveforms do not track as closely and cross-regulation in DCM is degraded compared to the case of near-ideal coupling. Fig. 10 shows the experimental waveforms observed with the coupled-inductor design #1 where winding W3 is coupled moderately well to W1 and W2. The winding W3 output operates in the DCM. The analysis of Section 3 predicts that the load resistance at the DCM/CCM boundary is $2l_3f_s/(1-\alpha_3)/(1-D) = 14\Omega$, which agrees well with the experimentally observed threshold resistance of 17Ω.

Fig. 11 compares the cross-regulation of the winding 2 and 3 outputs using the coupled-inductor design #1. It can be observed that cross-regulation is degraded compared to the near-ideal coupling case in the range of load currents where the winding W3 output operates in DCM.

4.3 The Zero-Ripple Approach

In this case, the series inductances are moderate or high in value and the effective turns ratios differ significantly from the

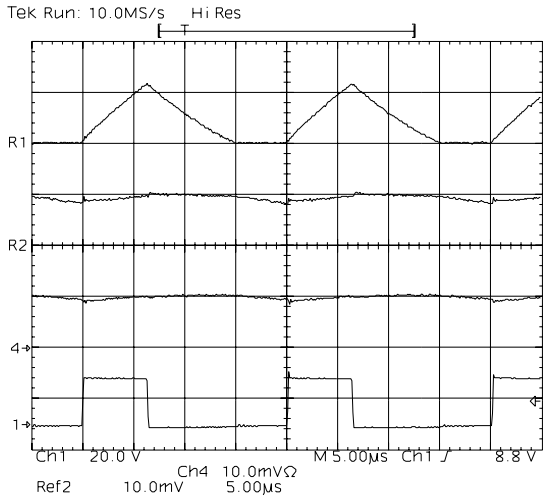

Figure 10: Waveforms in the experimental circuit using the coupled-inductor design #1; top-to-bottom: (R1) i_3 (0.5A/div); (R2) i_2 (1A/div); (4) i_1 (2A/div); (1) v_{s3} (20V/div). Operating conditions: $V_{o1} = 5.1$V, $I_{o1} = 2$A, $V_{o2} = 5.3$V, $I_{o2} = 0.97$A, $V_{o3} = 5.6$V, $I_{o3} = 0.2$A, $V_g = 20$V.

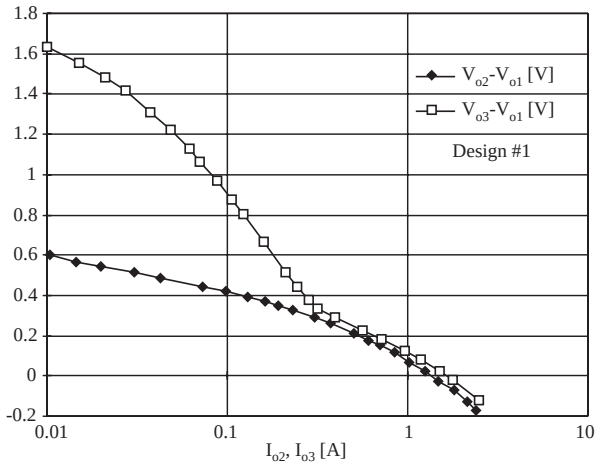

Figure 11: Experimental cross-regulation $(V_{o2}-V_{o1})(I_{o2})$ at $I_{o1} = 2$A, $I_{o3} = 1$A, and $(V_{o3} - V_{o1})(I_{o3})$ at $I_{o1} = 2$A, $I_{o2} = 1$A, using the coupled-inductor design #1.

physical turns ratios. By changing the number of turns, the effective turns ratio for an output can be adjusted to match the ratio of the voltages imposed on the windings by the converter. This results in $\alpha_j = 1$, which, as shown by the analysis of Section 3, implies that the winding current ripple is ideally zero and that the CCM operation is guaranteed for all loads. In general, the zero-ripple condition can be achieved in all but one winding. To do so, one simply needs to adjust the effective turns ratios to match the applied voltages, $n_j = N_j$, for all windings. In this case, the general condition $\alpha_j = 1$ is in equivalent to the "zero-ripple" condition discussed in [7].

In the experimental circuit, the coupled-inductor design #2 is used to illustrate the zero-ripple approach. Experimental waveforms for the case when all outputs are in the CCM are shown in Fig. 9. Winding W3 output operates in the CCM at very light load with very small residual ripple, as opposed to the current i_2 of the tightly-coupled winding W2 that exhibits

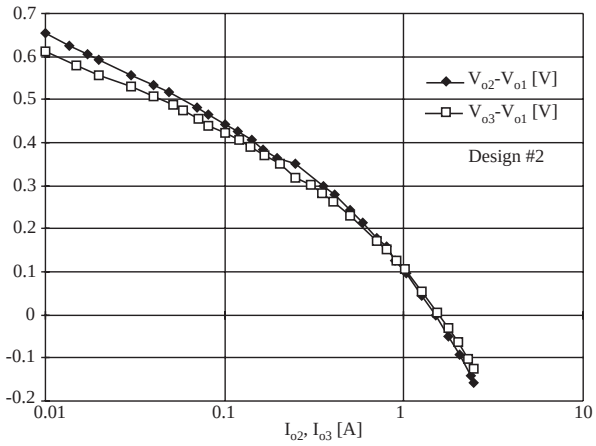

Figure 12: Experimental cross-regulation $(V_{o2}-V_{o1})(I_{o2})$ at $I_{o1} = 2$A, $I_{o3} = 1$A, and $(V_{o3} - V_{o1})(I_{o3})$ at $I_{o1} = 2$A, $I_{o2} = 1$A, using the coupled-inductor design #2.

large spikes. Measured cross-regulation results are shown in Figs. 12 for the case when the main output is operated in CCM. The cross-regulation on the winding W3 output is actually superior to the near-ideal coupling case because of the absence of circulating currents, and because the W3 output always operates in the CCM.

Since the windings are not tightly coupled in the zero-ripple approach, the winding voltage waveforms do not track closely; hence, cross-regulation is degraded if the non-zero-ripple outputs operate in DCM. This is illustrated by the waveforms of Fig. 13: outputs 1 and 2 are both in the DCM, while winding W3 output is in the CCM. The voltage v_{s3} differs significantly from the voltages v_{s1} and v_{s2}, the cross-regulation on the output 3 is degraded, and non-zero current ripple can be observed in the winding W3 current. The cross-regulation results for the outputs 2 and 3 obtained when the main output load current is varied are shown in Fig. 14. In this case, the output 2 with W2 tightly-coupled to the main-output winding W1 outperforms the output 3.

It can be concluded that the best cross regulation can be obtained via the zero-ripple approach in applications where there is at least one output whose load current variations are not too great: all of the ripple can be steered to this output, and all windings can always operate in CCM.

4.4 Dynamic Response Considerations

Coupled inductors, and the discontinuous conduction mode, can also significantly affect the converter small-signal dynamics. The extended cantilever model can be used to investigate dynamic responses of multiple-output converters by analytical tools or by simulation. A brief qualitative summary is presented in this section.

The leakage inductances of the extended cantilever model, in conjunction with the capacitances of the auxiliary outputs, can introduce resonances into the converter control-to-main-output transfer function. To mitigate these resonances, it may be necessary to reduce the leakage inductances via tight coupling. Furthermore, lower leakage inductances result in better dynamic cross-regulation, simply because the output

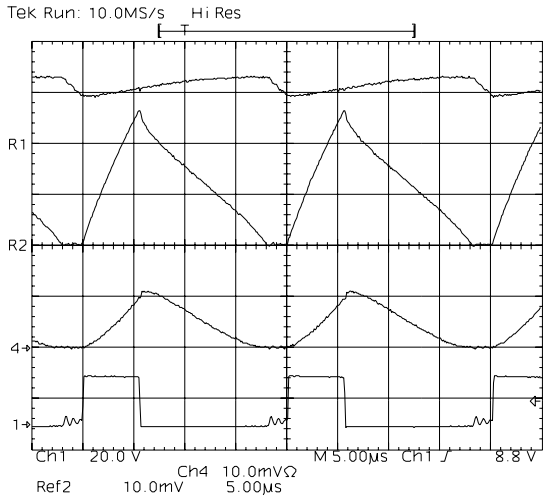

Figure 13: Waveforms in the experimental circuit using the coupled-inductor design #2; top-to-bottom: (R1) i_3 (200mA/div); (R2) i_2 (200mA/div); (4) i_1 (200mA/div); (1) v_{s1} (20V/div). Operating conditions: $V_{o1} = 5.1$V, $I_{o1} = 90$mA, $V_{o2} = 4.98$V, $I_{o2} = 230$mA, $V_{o3} = 4.81$V, $I_{o3} = 230$mA, $V_g = 20$V.

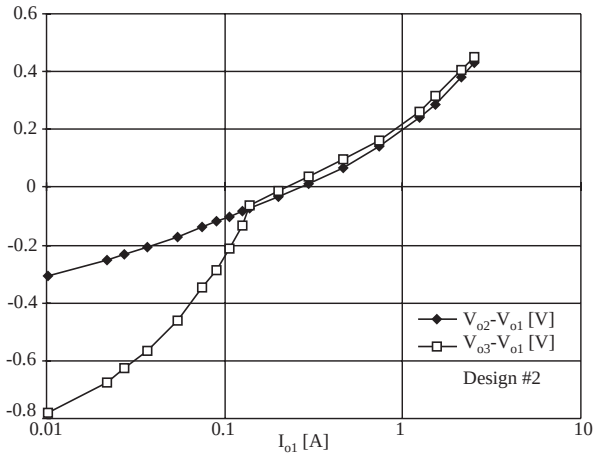

Figure 14: Experimental cross-regulation $(V_{o2} - V_{o1})(I_{o1})$ and $(V_{o3} - V_{o1})(I_{o1})$ for $R_{o2} = R_{o3} = 25\Omega$, $V_{o1} = 5.1$V.

impedances of the auxiliary outputs are smaller [4].

We have also observed significant changes in the control-to-main-output transfer function of a current-programmed forward converter with moderate coupling of inductors, when an auxiliary output enters the discontinuous conduction mode. This behavior can be explained as follows. The high-frequency asymptote of the current-programmed control-to-output transfer function depends on the total effective capacitance $C_{\rm tot}$. When all outputs operate in the continuous conduction mode, then $C_{\rm tot}$ is equal to the parallel combination of all output capacitors, referred to the main output. However, when a moderately-coupled output enters the discontinuous conduction mode, then the influence of its output capacitance on the control-to-main-output transfer function is greatly reduced. Depending on the relative values of the output capacitances, this effect can lead to significant variations in the crossover frequency of the main voltage feedback loop. This effect can be mitigated by choosing the output capacitance of the main output to be much greater than the reflected capacitances of the auxiliary outputs, or by obtaining near-ideal coupling of the inductor windings. This point is discussed further in [9].

5 Conclusions

A general extended cantilever model of the multiple-winding coupled inductor is described, in which all parameters can be directly measured. This model is employed in a tutorial explanation of the mechanisms by which leakage inductances and effective turns ratios affect cross regulation and discontinuous conduction mode boundaries in a multiple-output converter. Three basic approaches to coupled-inductor design are compared. Near-ideal coupling provides good cross-regulation even when some outputs become discontinuous; however, realization of near-ideal coupling may be difficult in practice, and the resulting circulating currents can also lead to increased output voltage ripples and reduced efficiency. Practical moderate coupling leads to lower circulating currents, but the cross regulation is degraded in discontinuous modes because the inductor waveforms are not matched as closely as in the near-ideal coupling case. In applications where there is at least one output whose load current variations are relatively small so that all winding can always operate in CCM, the best static cross regulation can be obtained via the zero-ripple approach with relatively loose coupling.

References

[1] S.Hsu, "Problems in analysis and design of switching regulators," Ph.D. Thesis, California Institute of Technology, 1979.

[2] M.Goldman, A.F.Witulski, "Predicting regulation for a multiple-output current-mode controlled DC-to-DC converter," IEEE PESC 93, pp.617-623.

[3] L.H.Dixon, Jr., "The effects of leakage inductance on switching power supply performance," Unitrode Power Supply Design Seminar, 1990, pp.P2.1-2.7.

[4] "Coupled filter inductors in multiple output buck regulators provide dramatic performance improvement," Unitrode Power Supply Design Seminar, 1990, pp.M7.1-7.10.

[5] A.Dauhajre, R.D.Middlebrook, "Modeling and estimation of leakage phenomena in magnetic circuits," IEEE PESC 1986.

[6] G.W.Ludwig, S.El-Hamamsy, "Coupled inductance and reluctance models of magnetic components," IEEE Trans. on Power Electronics, Vol.6, No.2, April 1991, pp.240-250.

[7] S. Ćuk, Z. Zhang, "Coupled-Inductor Analysis and Design," IEEE PESC 86, pp. 655-665.

[8] N. Jayaram and D. Maksimovi'c, "Power factor correctors based on coupled-inductor Sepic and Ćuk converters with nonlinear-carrier control," IEEE APEC 1998.

[9] D. Maksimović, "Automated small-signal analysis of switching converters using a general-purpose time-domain simulator," IEEE APEC 1998.